



## Ultra-pure hydrogen production from reformate mixtures using a palladium membrane reactor system

Mitra Abdollahi<sup>a</sup>, Jiang Yu<sup>a</sup>, Paul K.T. Liu<sup>b</sup>, Richard Ciora<sup>b</sup>, Muhammad Sahimi<sup>a</sup>, Theodore T. Tsotsis<sup>a,\*</sup>

<sup>a</sup> Mork Family Department of Chemical Engineering and Material Science, University of Southern California, Los Angeles, CA 90089-1211, USA

<sup>b</sup> Media and Process Technology Inc., Pittsburgh, PA 15328, USA

### ARTICLE INFO

#### Article history:

Received 7 May 2011

Received in revised form 4 October 2011

Accepted 21 October 2011

Available online 17 November 2011

#### Keywords:

Hydrogen production

Membrane reactor (MR)

Palladium (Pd) membrane

Water–gas shift reaction (WGS)

Fuel cell

### ABSTRACT

Hydrogen is considered today as a promising fuel of the future in order to address the existing environmental concerns associated with the use of fossil fuels. Hydrogen PEM fuel cells are an important enabling technology for this purpose, but their operating temperature is typically low and, as a result, common impurities found in conventional hydrogen production like CO, can adsorb on and poison the catalysts utilized. Therefore, high-purity hydrogen is required for the operation of such systems. In this study a realistic size, ultra-permeable Pd membrane is used for pure hydrogen production from a feed with a simulated reformate composition through the water gas shift (WGS) reaction. Prior to its use in the reactor experiments, the membrane is characterized through single-gas permeation measurements. The effect of feed pressure and flow rate and sweep ratio on membrane performance during the WGS experiments is experimentally studied, and the results are compared with those of a mathematical model. The model is further used to study the design aspects of the process. It is shown that the Pd membrane reactor system under study is capable of attaining almost complete CO conversion and full hydrogen recovery at realistic experimental conditions akin to those utilized in industrial applications.

© 2011 Elsevier B.V. All rights reserved.

### 1. Introduction

Fuel cells are widely considered as a clean and energy-efficient technology that shows promise as a future potential replacement for the internal-combustion (IC) engines in vehicles, IC engines and gas turbines in stationary power generation, and for batteries in portable power applications [1]. Proton-exchange membrane (also known as polymer electrolyte membrane or PEM) fuel cells are particularly promising as they are compact and lightweight units that work at comparatively lower temperatures and pressures, which makes them good candidates for use in mobile and small-scale distributed stationary power generation applications. PEM fuel cells make use of a thin, permeable polymeric membrane as the electrolyte, and platinum (Pt) electrodes are used on either side of the membrane in order to catalyze the reactions. Hydrogen is typically utilized as the fuel and is fed to the anode, where it catalytically splits into protons (which transport through the membrane to the cathode) and electrons that travel along an external load circuit to the cathode, thus producing electricity. Oxygen (as air) is simultaneously supplied to the cathode, where it combines with the hydrogen ions to produce water [2].

The hydrogen, that PEM fuel cells need to operate, can be produced from different renewable (e.g., water, biomass) and non-renewable (e.g., fossil fuels) feed-stocks through various processes [3,4]. Due to its higher efficiency, currently steam methane reforming (SMR) is the primary industrial process that is used for H<sub>2</sub> production. In SMR, steam reacts with methane at high temperatures and pressures in the presence of a catalyst to produce hydrogen according to the following reaction:



CO that is simultaneously produced as an undesirable by-product of SMR is known to be particularly detrimental for PEM fuel cell operation. Even when present at trace concentrations in the H<sub>2</sub> stream, CO is reported to degrade PEM fuel cell performance as it severely poisons the electro-active Pt surface in the anode, thus preventing H<sub>2</sub> oxidation. The tolerance of PEM fuel cells to CO depends on the material used for preparing the anode, with most studies reporting an acceptable level of 10 ppm or less. Substantially higher tolerances have been reported as well. Pt–Ni/C, for example, is reported to be tolerant to up to 50 ppm of CO [5], while Pt–Ru supported on defect-free carbon nano-tubes has been reported capable to tolerate up to 100 ppm of CO [6].

For the hydrogen produced from SMR to be utilized in PEM fuel cells, care must, therefore, be paid towards decreasing its CO content prior to entering the fuel cell stack. Typically, the first step

\* Corresponding author. Tel.: +1 213 740 2069; fax: +1 213 740 8053.

E-mail address: [tsotsis@usc.edu](mailto:tsotsis@usc.edu) (T.T. Tsotsis).

involves utilizing the water gas shift (WGS) reaction (see below) in tandem with the SMR in order to react the CO in the reformate mixture and to produce additional H<sub>2</sub>.



Conventional WGS reactors can attain high CO conversions, but not to the degree required to prevent CO-induced PEM fuel cell stack performance degradation. This, then, means that following the H<sub>2</sub>/CO<sub>2</sub> separation step (e.g., via pressure swing adsorption (PSA)) an additional CO removal step must be implemented involving either the catalytic oxidation of CO (this is known as preferential oxidation or PROX, Eq. (3)) or methanation (Eq. (4)) in order to reduce the CO level into the acceptable fuel cell operational range.



Both approaches, unfortunately, end-up consuming part of the H<sub>2</sub> (since in the presence of oxygen some catalytic oxidation of the hydrogen is unavoidable). Methanation offers more simplicity than PROX, since no oxygen needs to be added to the reactor. On the other hand, it typically results in higher hydrogen consumption for the same CO conversion. For either process, the lower the CO content is, the less hydrogen is consumed and the more efficient the process is. Therefore, it is highly desirable to be able to produce either pure H<sub>2</sub> or a H<sub>2</sub> product with an acceptable CO content, which does not require sacrificing part of hydrogen, during further purification, and increasing process complexity.

The above conventional SMR+WGS+PSA+PROX (or methanation) system is one of significant complexity. To add to this complexity, since WGS is an equilibrium-limited reaction, usually two reactors are utilized: one operating at high temperatures (high-temperature shift or HTS), and the other at low temperatures (low-temperature shift or LTS) in order to maximize the CO conversion. In order to improve process efficiency and to minimize system complexity, membrane reactors (MR) are employed for the WGS reaction. These reactors combine reaction and separation in one unit, and in the context of their application to pure hydrogen production provide many advantages. By removing hydrogen from the reactor, for example, conversion increases and less steam is required. CO<sub>2</sub> is separated in the reject side at high pressure, thus eliminating the need for using a separate PSA unit. With highly permselective membranes the need for using a separate PROX or methanation step may be completely eliminated, but even for less permselective membranes the overall system efficiency for the PROX (or the methanation) step improves, and hydrogen loss is minimized. Even the use of inexpensive, low-pressure steam as a sweep for the permeate side of these WGS-MR may provide an advantage, as it generates a pre-humidified H<sub>2</sub> product as a feed, which is a requirement for many PEM fuel cell stack applications.

Membrane reactors have been used for both the SMR [7,8] and the WGS reactions [9–17] for H<sub>2</sub> production. Due to the high process temperatures required, metal membranes like Pd and its alloys [9–13], inorganic membranes like microporous silica [14], and carbon molecular sieve (CMS) membranes [15–17] have all been utilized. CMS membranes provide a great advantage for the WGS application in the context of integrated gas combined cycle (IGCC) applications for coal and biomass, as they are very robust to the various impurities (e.g., H<sub>2</sub>S, NH<sub>3</sub>, tar, etc.) one, typically, encounters in such systems. These impurities are highly detrimental to the mechanical stability of the metal membranes. Pd and Pd-alloy membranes are, however, well-suited for high-purity hydrogen production via the use of SMR for fuel cell applications, due to their very high (in principle, infinite) selectivity towards hydrogen. As a result, a number of groups have investigated their application for hydrogen production. Jansen et al. [18], for example, performed a

techno-economic analysis of two process schemes involving the use of Pd membrane reactors integrated in natural gas-based combined power generation cycles. These include (a) a process utilizing a WGS, and (b) one utilizing an SMR membrane reactor. The cycle involving the use of the WGS membrane reactor proved to provide higher efficiency and lower capital cost. Jansen et al. [18] attributed this to the fact that the typical feed to an SMR unit contains methane and steam, with little or no H<sub>2</sub> being present. The WGS feed, on the other hand, contains considerable amounts of H<sub>2</sub>, which are produced during the SMR reaction. Thus, when using the Pd membrane for the WGS step, since the driving force for H<sub>2</sub> transport across the membrane is higher, less membrane area is required. Jansen et al. [18] also note that SMR reactors, typically, operate at much higher temperatures when compared to their WGS counterparts. High temperature has a negative impact on Pd membrane stability due to accelerated membrane degradation; to counteract this impact one may have to utilize thicker membranes, thus increasing the membrane cost, but more importantly also reducing the H<sub>2</sub> flux.

A number of researchers have studied the use of Pd membranes for the WGS reaction. Basile et al. [9] used Pd and Pd/Ag membranes for the WGS reaction, and reported conversion values higher than thermodynamic equilibrium. They used a model WGS feed to their reactor which contained no inert or other reaction products one would normally expect to find in a typical reformate mixture, and for simplicity they utilized nitrogen as sweep. Iyoha et al. [10] performed the WGS reaction in the absence of any catalyst at a temperature of 900 °C and an operating pressure of 2.41 bar making use of Pd and Pd-alloy (80 wt% Pd–20 wt% Cu) tubular membranes. The high rate of hydrogen extraction through the Pd-based membranes resulted in increasing the carbon monoxide conversion to 93%. The conversion decreased from 93% to 66% and hydrogen recovery from 90% to 85% when the Pd membranes were replaced with the Pd–Cu ones, which Iyoha et al. [10] attributed to the lower permeance of the Pd–Cu alloy membranes. Though the study of Iyoha et al. [10] provides the advantage of not needing to use a catalyst, the long-term mechanical stability of these materials at these extremely high temperatures raises concerns.

Bi et al. [11] used a Pt/Ce<sub>0.6</sub>Zr<sub>0.4</sub>O<sub>2</sub> HTS catalyst with a highly H<sub>2</sub>-permeable and selective Pd/ceramic composite membrane in a WGS membrane reactor, 4.9 cm in length and 1.4 cm in diameter. Unlike the previous studies, Bi et al. [11] utilized a simulated reformate mixture (45.3% H<sub>2</sub>, 11.8% CO, 34.4% H<sub>2</sub>O, 7.4% CO, 1.1% CH<sub>4</sub>). The system provided CO conversions above thermodynamic equilibrium at T = 350 °C, P = 12 bar and H<sub>2</sub>O/CO = 3, and showed a sharp decline in H<sub>2</sub> recovery with increasing gas hourly space velocity under these conditions. The highest reported H<sub>2</sub> purity by the system was 99.7%. Interestingly, though their catalyst had a substantial methanation activity under packed-bed reactor conditions (especially in comparison with the more conventional Fe–Cr HTS catalyst), its methanation activity significantly diminished in the MR (this is consistent with the findings of this study, whereby very little if any methanation activity is observed during MR operation).

Mendes et al. [12] recently studied the performance of a Pd–Ag membrane reactor for the WGS reaction using a Cu–Zn LTS catalyst. A dense metallic permeator tube (5 cm in length, and 1 cm in internal diameter) was assembled from a commercial flat sheet of Pd–Ag. The catalyst was packed in the membrane lumen. A simulated reformate feed composition (4.7% CO, 34.78% H<sub>2</sub>O, 28.70% H<sub>2</sub>, 10.16% CO<sub>2</sub>, balanced with N<sub>2</sub>) was utilized. The MR performance was evaluated in terms of CO conversion and H<sub>2</sub> recovery at different experimental conditions, e.g., different temperatures (200–300 °C), pressures (1–4 bar), and using either vacuum (30 mbar) or N<sub>2</sub> as a sweep stream. The MR delivered CO conversions above the thermodynamic equilibrium in most of the cases, but hydrogen recoveries were rather low (except in the case of using vacuum). No data were

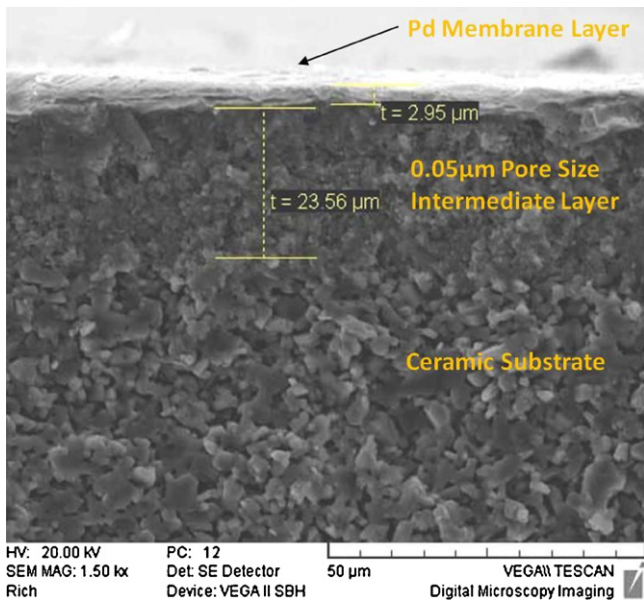


**Fig. 1.** SEM cross-section of the Pd layer deposited on the alumina support using the ELP method.

presented for the permselectivity of the membrane or for the purity of the hydrogen product.

Though some preliminary work on the use of Pd membranes for the WGS reaction has already been presented, most of the studies to date (with a couple of notable exceptions) have utilized pure feeds and not the typical reformate compositions, which in addition to CO contain substantial amounts of H<sub>2</sub> and CO<sub>2</sub>. In addition, typically, vacuum or inert gas is utilized as the sweep, which is unlikely to be the case in the commercial case as it will entail substantial additional costs for recompression (when using high vacuum) or purification of the hydrogen product (when using nitrogen as the sweep). The membranes, furthermore, were of a small laboratory size. In this study, we investigate instead the use of “commercial-scale” Pd membranes, prepared via electroless plating (ELP) on 0.05 μm pore size asymmetric tubular Media and Process Technology, Inc. (M&P) commercial ceramic substrates (Fig. 1 shows a typical SEM cross-section of the Pd membranes prepared by our team). Realistic feeds with a simulated reformate composition are being used in our study, together with steam as a sweep. The membrane reactor performance is investigated at different feed pressures and flow rates, and steam sweep ratios. The experimental results are compared with the simulation results from a mathematical model. The model is further used to study the effect of experimental conditions on CO conversion, H<sub>2</sub> recovery and purity of the hydrogen product.

## 2. Experimental procedure

A schematic of the experimental set-up used in this study is shown in Fig. 2. A tubular Pd membrane ( $L = 762$  mm, ID = 3.5 mm, OD = 5.7 mm), is utilized which is prepared by depositing a thin Pd layer via the ELP technique on a 0.05 μm pore size asymmetric, tubular mesoporous commercial M&P alumina support. During preparation, the M&P porous  $\alpha$ -Al<sub>2</sub>O<sub>3</sub> tubes are cut into the appropriate length, rinsed and dried. The activation and Pd deposition procedure follows the conventional technique previously described in the technical literature [19]. In short, the tubes are activated by dipping them into the Pd acetate solution for 1 min, and then dried and calcined. The substrate, thus activated, is then plated at room temperature by immersing it in the electroless Pd plating bath with

the composition as described in [19]. As expected, the thickness of the Pd layer is dependent on the time of deposition, being ~3 μm for the membranes used in this study. Upon completion of the electroplating step, the supported membranes are rinsed in distilled water overnight, and are then dried, to be ready for use. The supported Pd membrane is inserted inside a stainless steel (SS) reactor and sealed with the aid of O-rings and compression fittings. Graphite O-rings are used for sealing both ends of the membrane, along with SS washers/shims as back-stops to prevent the graphite from extruding into the catalyst bed. A schematic illustration of the membrane module is also shown in Fig. 2.

A commercial, low-temperature Cu-Zn/Al<sub>2</sub>O<sub>3</sub> (44% CuO, 44% ZnO, balance Al<sub>2</sub>O<sub>3</sub>) catalyst is utilized. The catalyst particles are crushed into smaller pieces, and a fraction of the particles with sizes in the range of 600–800 μm is selected, using sieving trays; they are then mixed with crushed quartz particles (in the same size range) and loaded into the annular space in between the membrane and the reactor wall. The reason for diluting the catalyst with inert quartz particles is so that the reactor volume is completely filled (to avoid flow channeling), but also in order to assure isothermality along the reactor length.

The reactor is heated by means of a six-zone furnace, using six temperature controllers connected to six thermocouples installed at different locations along the length of the bed. To verify reactor isothermality, an additional thermo-well is installed in the catalyst bed, and is used to monitor the temperature along the length of the reactor with the aid of a sliding thermocouple. Reactor feeds with compositions simulating those at the exit of a reformer (e.g., containing H<sub>2</sub>, CO, CO<sub>2</sub> and CH<sub>4</sub>) are prepared using mass flow controllers. The steam flows for the reactant feed and the sweep streams are provided by steam generators; these are SS vessels packed with quartz beads in order to accelerate water evaporation, and to dampen out any fluctuations in the flow of the steam. The steam generators are wrapped with heating tapes and insulated, and during operation their temperatures are controlled via the use of individual temperature controllers. Controlled flows of water into the steam generating units are provided by syringe pumps. All lines (including the feed, sweep, reject and permeate), are heat-traced via the use of heating tapes and insulation. In order to monitor the pressure, gauges are installed in all the lines. Needle valves are utilized in the reject and permeate lines in order to adjust and to control the pressure.

During the membrane reactor experiments, the reactant feed is preheated to the reactor temperature and directed towards the catalyst bed, where the WGS reaction takes place. Steam, used as a sweep, is directed towards the membrane permeate side. The gas that transports through the Pd membrane (H<sub>2</sub>) passes through the membrane and exits the reactor through the permeate line, while unreacted gases and other products (CO<sub>2</sub>) exit through the reject side. Upon exiting the reactor, permeate and reject streams pass first through condensers, and then through the moisture traps in order to remove any water that remains. The flow rates of the water-free streams are then measured using bubble flow-meters. Small slip-streams from both the permeate and reject streams are directed towards a gas chromatograph, where their compositions are measured. Single-gas permeation measurements are carried out before the initiation of the MR experiments in order to characterize the membrane transport characteristics, as well as after the experiments are completed in order to validate the membrane stability. No sweep gas is utilized in these experiments.

## 3. Mathematical model

An isothermal co-current membrane reactor model, previously developed by our group [20], is used to describe the reactor

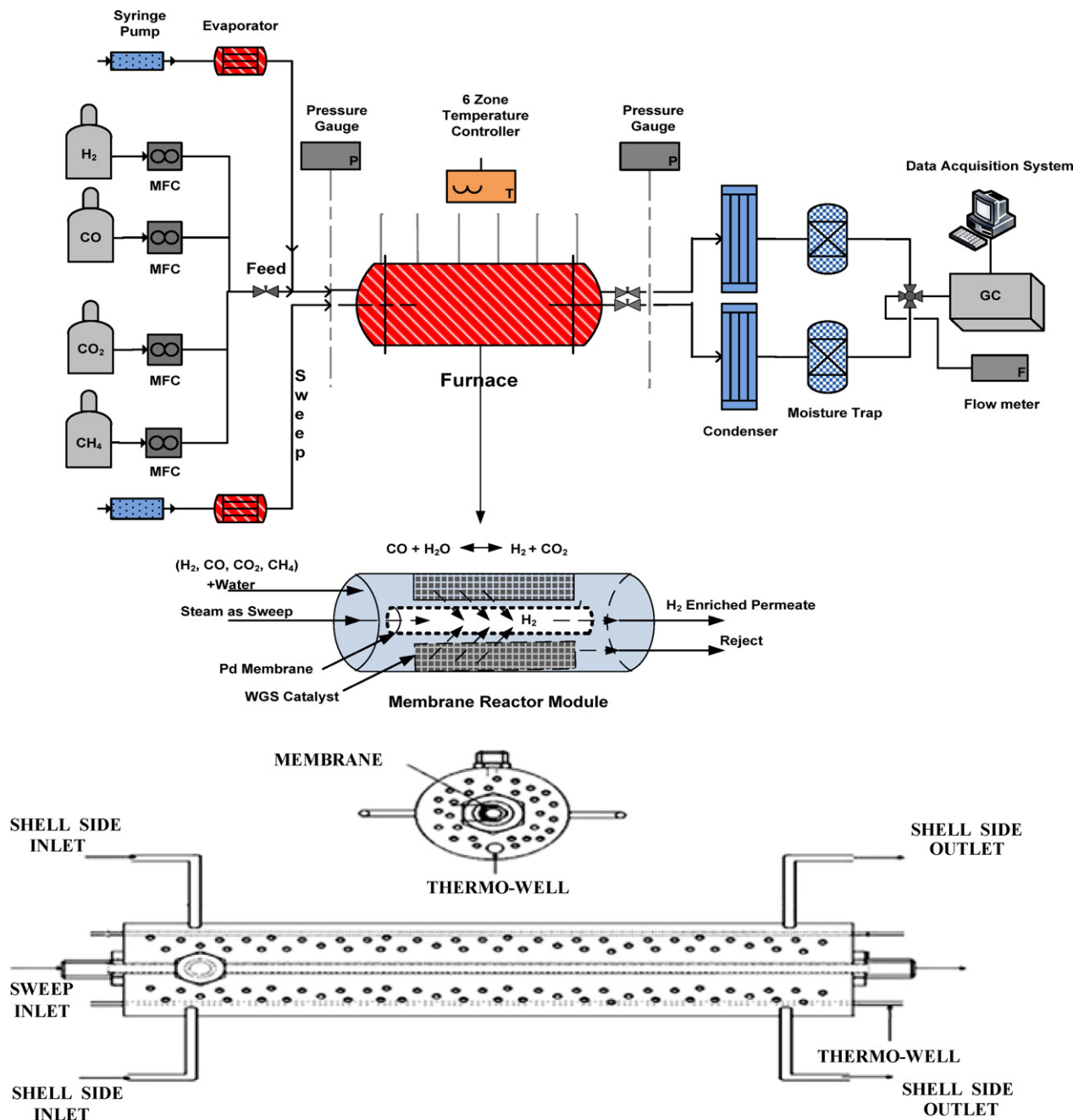


**Fig. 2.** The experimental set-up and the membrane module.

performance. Hydrogen transport through the Pd membrane is described with the following empirical equation:

$$F_{H_2} = U_{H_2}((P_{H_2}^F)^n - (P_{H_2}^P)^n) \quad (5)$$

where  $F_{H_2}$  is the  $H_2$  molar flux ( $\text{mol}/\text{m}^2 \text{ h}$ ),  $P_{H_2}^F$  (bar) the  $H_2$  partial pressure in the feed side,  $P_{H_2}^P$  (bar) the  $H_2$  partial pressure in the permeate side,  $n$  the pressure exponent, and  $U_{H_2}$  ( $\text{mol}/\text{m}^2 \text{ h bar}^n$ ) the  $H_2$  permeance.

Ideally, Pd membranes would allow only hydrogen to permeate through. In reality, often small cracks and defects develop which permit small amounts of other gases to permeate through. In the model, membrane mass transport for species other than  $H_2$  is described as follows:

$$F_j = U_j(P_j^F - P_j^P) \quad (6)$$

where  $F_j$  is the molar flux for component  $j$  ( $\text{mol}/\text{m}^2 \text{ h}$ ),  $P_j^F$  (bar) the partial pressure for component  $j$  in the feed side,  $P_j^P$  (bar) the partial pressure for component  $j$  in the permeate side, and  $U_j$  ( $\text{mol}/\text{m}^2 \text{ h bar}^n$ ) the permeance for component  $j$ .

$H_2$  mass balances in the feed and permeate sides are described by Eqs. (7) and (8), respectively.

$$\frac{dn_{H_2}^F}{dV} = -\alpha_m U_{H_2}((P_{H_2}^F)^n - (P_{H_2}^P)^n) + (1 - \varepsilon_v)\beta_c \rho_c r^F \quad (7)$$

$$\frac{dn_{H_2}^P}{dV} = \alpha_m U_{H_2}((P_{H_2}^F)^n - (P_{H_2}^P)^n) \quad (8)$$

where  $n_{H_2}^F$  is the  $H_2$  molar flow rate ( $\text{mol}/\text{h}$ ) in the feed side,  $n_{H_2}^P$  the corresponding molar flow rate ( $\text{mol}/\text{h}$ ) in the permeate side,  $V$  the reactor volume variable ( $\text{m}^3$ ),  $\alpha_m$  the surface area of the membrane

**Table 1**

Pressure-dependence of hydrogen transfer through palladium and palladium-alloy membranes.

| Membrane                             | Temperature (°C) | Synthesis method  | Pd layer thickness (μm) | Pressure exponent (n) | Ref. |
|--------------------------------------|------------------|---|-------------------------|-----------------------|------|
| Pd                                   | 350              | –   | 24–154                  | 0.68                  | [22] |
| Pd                                   | 350–900          | Punching circular disks out of a 1-mm thick palladium sheet | 1000                    | 0.5–0.62              | [23] |
| Pd/Al <sub>2</sub> O <sub>3</sub>    | 300–500          | Metal-organic chemical vapor deposition                     | 2                       | 1                     | [24] |
| Pd/Al <sub>2</sub> O <sub>3</sub>    | 450              | Electroless plating   | 5–8                     | 1                     | [25] |
| Pd/Al <sub>2</sub> O <sub>3</sub>    | 250–450          | Electroless plating   | 5–8                     | 0.75                  | [26] |
| Pd–Ag                                | 350              | Electron beam evaporation of Ag on commercial Pd foil       | 25                      | 1                     | [27] |
| Pd–Ag/Al <sub>2</sub> O <sub>3</sub> | 400              | Electroless plating   | 20                      | 0.76                  | [28] |
| Pd–Ag/Al <sub>2</sub> O <sub>3</sub> | 350–500          | Electroless plating   | 8.6                     | 0.5                   | [29] |
| Pd–Ag/glass                          | 200–400          | Magnetron sputtering of Pd–Ag on glass support              | 6.8                     | 0.5                   | [30] |
| Pd–Cu/zirconia coated alumina        | 350–450          | Electroless plating   | 1–11                    | 0.52–1                | [31] |

per unit reactor volume (m<sup>2</sup>/m<sup>3</sup>),  $\varepsilon_v$  the bed porosity in the feed side,  $\beta_c$  the fraction of the solid volume occupied by the catalysts,  $\rho_c$  the catalyst density (g/m<sup>3</sup>), and  $r^F$  the WGS reaction rate (mol/g h).

Mass balances for components other than H<sub>2</sub> in the feed and permeate sides are described by Eqs. (9) and (10), respectively.

$$\frac{dn_j^F}{dV} = -\alpha_m U_j (P_j^F - P_j^P) + v_j (1 - \varepsilon_v) \beta_c \rho_c r^F \quad (9)$$

$$\frac{dn_j^P}{dV} = \alpha_m U_j (P_j^F - P_j^P) \quad (10)$$

where  $n_j^F$  is the molar flow rate (mol/h) for component  $j$  in the feed side,  $n_j^P$  the corresponding molar flow rate (mol/h) in the permeate side, and  $v_j$  is the stoichiometric coefficient for component  $j$ , negative for reactants and positive for products.

The pressure drop in the packed-bed is calculated using the Ergun equation (Eqs. (11)–(13), below).

$$-\frac{dP^F}{dV} = 10^{-6} \frac{f(G^F)^2}{A^F g_c d_p \rho^F} \quad (11)$$

$$f = \left[ \frac{1 - \varepsilon_v}{\varepsilon_v^3} \right] \left[ 1.75 + \frac{150(1 - \varepsilon_v)}{N_{Re}^F} \right] \quad (12)$$

$$N_{Re}^F = \frac{d_p G^F}{\mu^F} \quad (13)$$

where  $P^F$  is the feed-side pressure (bar),  $A^F$  the cross-sectional area available to flow for the reactor feed side (m<sup>2</sup>),  $\mu^F$  the viscosity (g/m h),  $d_p$  the particle diameter in the feed side (m),  $G^F = \rho^F \mu^F$ , the superficial mass flow velocity in the feed side (g/m<sup>2</sup> h),  $u^F$  the average velocity of the fluid (m/h),  $\rho^F$  the average fluid density (g/m<sup>3</sup>), and  $g_c$  the gravity conversion factor.

The above set of equations are solved numerically together with the following boundary conditions (Eq. (14)):

$$\text{At } V = 0 : n_j^F = n_{j0}^F, \quad n_j^P = n_{j0}^P, \quad P^F = P_0^F, \quad P^P = P_0^P \quad (14)$$

where  $P_0^F$  is the inlet feed-side pressure (bar),  $P_0^P$  is the inlet permeate-side pressure (bar) and  $n_{j0}$  is the inlet molar flow rate for component  $j$  (mol/h). Finally, Eqs. (15) and (16) are used to calculate the CO conversion and H<sub>2</sub> recovery, as follows:

$$X_{CO} = \frac{n_{COo}^F - (n_{CO,exit}^F + n_{CO,exit}^P)}{n_{COo}^F} \quad (15)$$

$$Re_{H_2} = \frac{n_{H_2,exit}^P}{(n_{H_2,exit}^F + n_{H_2,exit}^P)} \quad (16)$$

where  $n_{COo}^F$  is the CO molar flow rate at the inlet (mol/h),  $n_{CO,exit}^F$  the CO molar flow rate at the exit of the reactor's feed side (mol/h),

$n_{CO,exit}^P$  the CO molar flow rates at the exit of the reactor's permeate side (mol/h),  $n_{H_2,exit}^F$  the hydrogen molar flow rate at the exit of the reactor's feed side (mol/h), and  $n_{H_2,exit}^P$  is the hydrogen molar flow rate at the exit of the reactor's permeate side (mol/h) (inherent in Eq. (15) is the assumption that the steam sweep in the permeate side contains no CO impurities).

## 4. Results and discussion

### 4.1. Membrane characterization

As noted previously, hydrogen transport through Pd and Pd-alloy membranes is commonly described by Eq. (5). The mechanism of hydrogen transport through Pd membranes is thought to involve the dissociative adsorption of hydrogen on the Pd surface on the feed-side, its diffusion through the metallic lattice, and recombination of the hydrogen atoms and desorption of hydrogen from the membrane surface on the permeate-side. In practical situations, external gas-phase mass transfer limitations as well transport limitations through the porous support, and diffusion and Poiseuille flow through membrane pinholes and cracks may also substantially affect H<sub>2</sub> permeation through composite Pd membranes [21]; the presence of various surface impurities that affect hydrogen adsorption/desorption on the Pd surface may also impact hydrogen permeation. For a clean, defect-free, thick Pd membrane at high temperatures (>300 °C), diffusion through the bulk metal is likely to be the rate limiting step, and the pressure exponent  $n = 0.5$  (Eq. (5) is then known as Sievert's law). However, for composite membranes prepared by depositing thin Pd films (<10 μm thick) on porous supports (as the membranes in this study), external mass transfer through the support layer can provide substantial added resistance to H<sub>2</sub> transport. The presence of impurities on the membrane surface and at the grain boundaries (as well mass transport through unavoidable defects) may also have substantial effects. In such instances, the  $n$  value ranges from 0.5 to 1, and should be obtained experimentally. Table 1, summarizes selected literature data on the pressure-dependence of hydrogen transport through Pd and Pd-alloy membranes [22–31]. As seen in the table, some studies report  $n$  values >0.5 even for membranes with thicknesses larger than 10 μm [22,23,27,28], and in one study for membranes as thick as 1 mm [23]. On the other end of the spectrum, other studies report  $n$  values equal to 0.5 for membranes which are thinner than 10 μm [29,30]. Clearly, the synthesis method which affects the physical and chemical structure of the final Pd membrane film has also a strong effect on the value of the exponent  $n$ .

Our group has extensively investigated the hydrogen transport through the ultra-long, ultra-thin Pd membranes, prepared by the electroless plating technique that are used in this study [25,26].

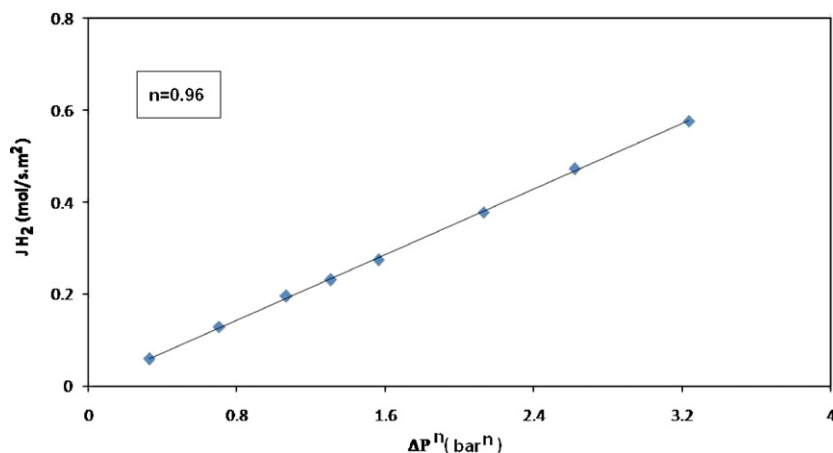


Fig. 3. Flux of hydrogen as a function of  $(P^F)^n - (P^P)^n$  at  $T = 300^\circ\text{C}$ .

Our results indicate that, depending on the preparation conditions,  $\text{H}_2$  transport through our Pd membranes obeys Eq. (5), with the exponent  $n$  ranging from 0.75 to 1. Fig. 3 shows single-gas  $\text{H}_2$  permeation data at  $T = 300^\circ\text{C}$  with one of the supported Pd membranes, prepared under identical conditions with the membrane used in the membrane reactor experiments in this study. The membrane permeation data are described well by Eq. (5), with the pressure exponent  $n = 0.96$ . Transport of gases, other than hydrogen, through our Pd membranes were found experimentally to obey Eq. (6) (i.e., the permeability is independent of pressure). During membrane synthesis, large defects and cracks sometimes develop that may result in convective flows; however, we have found their impact on performance to be so severe that such membranes are not selected for further study. The experimentally measured single-gas permeances of the membrane utilized in the MR experiments are shown in Table 3.

CO is known to affect  $\text{H}_2$  permeation through Pd and Pd-alloy membranes through its competitive adsorption on the membrane surface, especially at lower temperatures, which favor its adsorption [27]. For example, for a feed consisting of CO and  $\text{H}_2$ , almost no  $\text{H}_2$  permeation was reported in Pd membranes at temperatures below  $150^\circ\text{C}$  [27]. For temperatures of  $300^\circ\text{C}$  and above, however, the literature data are not in complete agreement. Some of the studies have shown that CO has almost no effect on the hydrogen permeation [27], while other studies report a decline in the hydrogen flux due to the presence of CO [32]. A direct comparison is unfortunately difficult to attain, as the membrane synthesis method and experimental conditions used (e.g., temperature, pressure, and feed composition) vary widely among the various studies.

We have, ourselves, studied experimentally the effect of CO on the  $\text{H}_2$  permeation rate through our Pd membranes at the conditions utilized in this study. In a series of experiments (with the membrane used in the MR experiments), the hydrogen flux through the membrane was first measured (at 2.02 bar and  $300^\circ\text{C}$ ) in a flowing pure hydrogen stream (6 mol/h), prior to exposing the membrane to CO. Then, the membrane was exposed to a flowing pure CO stream (at  $P = 1.01$  bar and  $T = 300^\circ\text{C}$ ) for different periods of time, ranging from 30 min to 5 h. Following exposure to CO, the feed was then switched back to pure hydrogen (same flow rate of 6 mol/h, at 2.02 bar), with the membrane temperature staying at  $300^\circ\text{C}$ ; the hydrogen permeation rate was then immediately measured (within 5 min from the gas atmosphere switch). Fig. 4 shows the experimental results in terms of the normalized  $\text{H}_2$  flux (defined as the ratio of the hydrogen flux immediately measured after membrane exposure to CO, to the starting membrane  $\text{H}_2$  flux). As shown in Fig. 4, there are no systematic trends in the data pointing to inhibition due to exposure to CO. The maximum difference between

the hydrogen flux of the fresh membrane and the flux measured after the membrane had been exposed to CO is 7.1%. Note, however, that for longer periods of exposure to CO (3 and 5 h) there are virtually no changes in the hydrogen flux upon exposure to CO. One can conclude from these observations that CO adsorbs rather weakly at  $300^\circ\text{C}$  on the particular Pd membrane used in this study, consistent with prior literature data.

We also include here additional experimental data (at  $300^\circ\text{C}$  and 3.08 bar) with a Pd membrane prepared under identical conditions with that in Fig. 4 (this membrane is shorter, 25.4 cm long, and its hydrogen permeance is 20% less than the membrane in Fig. 4, still however, within an acceptable quality tolerance for the synthesis of such membranes). In these experiments, the membrane is exposed to different mixed-gas, reformate-type feed compositions under sufficiently high feed flow conditions for which the partial hydrogen pressure difference between the feed and permeate sides at the exit of the membrane module is substantially non-zero (note that this is important for these high-flux membranes to avoid data falsification due to the fact that otherwise a large fraction of the membrane area may not be active in transport). Three different feed compositions were tested. The first feed composition (hereinafter referred to as Feed 1) corresponds to the reformate gas mixture used in the MR experiments (see further discussion to follow), namely  $\text{H}_2:\text{CO}:\text{CO}_2:\text{CH}_4:\text{H}_2\text{O} = 5.22:1:0.48:0.1:2.8$ . The second composition (Feed 2) is the same composition but on a “dry basis”, that is without any water being present, namely  $\text{H}_2:\text{CO}:\text{CO}_2:\text{CH}_4 = 5.22:1:0.48:0.1$ . The third feed composition (Feed 3) is  $\text{H}_2:\text{CO}:\text{CO}_2:\text{CH}_4:\text{H}_2\text{O} = 6.12:0.1:1.38:0.1:1.9$  corresponding to 90% CO conversion of the original composition (Feed 1). For each series of experiments the membrane was kept in the

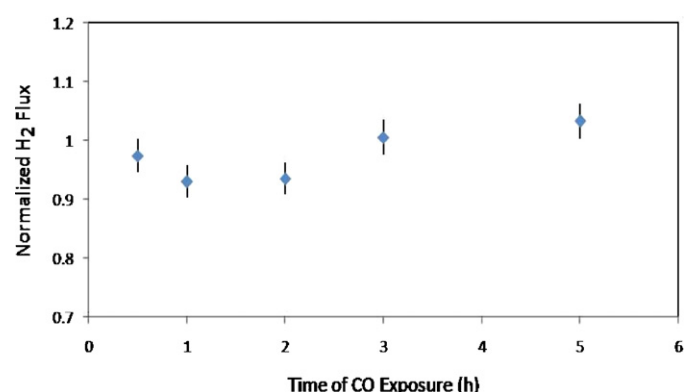
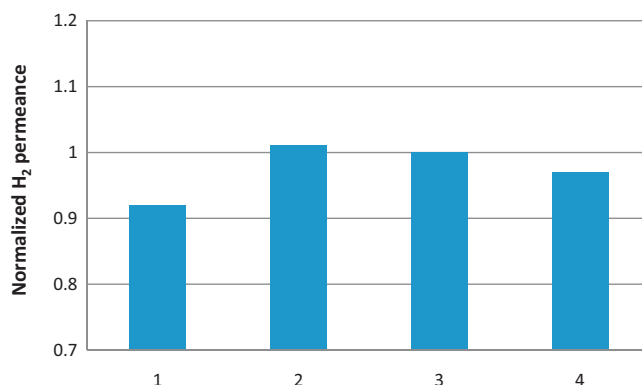


Fig. 4. Effect of CO on the membrane  $\text{H}_2$  permeation rate.

**Table 2**

Hydrogen permeance and selectivity of alumina supported palladium or palladium-alloy membranes prepared using the ELP method.

| Membrane   | Thickness (μm) | T (°C) | H <sub>2</sub> permeance (mol/m <sup>2</sup> s bar) | Separation factor                      | Ref. |
|--|----------------|--------|---|--|------|
| Pd/γ-Al <sub>2</sub> O <sub>3</sub>  | 6              | 480    | 0.260   | 2100 (H <sub>2</sub> /Ar)              | [34] |
| Pd/γ-Al <sub>2</sub> O <sub>3</sub> packed with yttria-stabilized zirconia | 5              | 450    | 0.125   | –                                      | [35] |
| Pd/γ-Al <sub>2</sub> O <sub>3</sub>  | 5              | 507    | 0.126   | 600 (H <sub>2</sub> /N <sub>2</sub> )  | [35] |
| Pd <sub>88</sub> Ag <sub>12</sub> /γ-Al <sub>2</sub> O <sub>3</sub>        | 11             | 550    | 0.121   | 2000 (H <sub>2</sub> /N <sub>2</sub> ) | [36] |
| Pd/γ-Al <sub>2</sub> O <sub>3</sub>  | 2.6            | 370    | 0.048   | 3000 (H <sub>2</sub> /N <sub>2</sub> ) | [37] |
| Pd/silicalite-1 zeolite  | 5              | 500    | 0.180   | 1300 (H <sub>2</sub> /N <sub>2</sub> ) | [38] |



**Fig. 5.** Normalized H<sub>2</sub> permeance for various feeds; Bar 1 for Feed 1, Bar 2 for Feed 2, Bar 3 for Feed 3, and Bar 4 for single-gas H<sub>2</sub> permeance measured after the mixed-gas experiments were completed.

corresponding feed composition for at least 4 h before measuring the flow rates and compositions of the reject and permeate sides. The mixed-gas hydrogen permeance was then calculated by fitting the experimental data using Eqs. (7) and (8) (without the reaction term), and compared with the single-gas permeance for hydrogen measured before and after the experiments. Fig. 5 shows the experimental results in terms of the normalized H<sub>2</sub> permeance (defined as the ratio of the mixed-gas hydrogen permeance divided by the starting single-gas H<sub>2</sub> permeance). Again, no systematic trends are observed pointing out any detrimental effects (at these relatively high temperatures and low total pressures) that relate to the presence of CO (or any other reformate mixture component) on the hydrogen permeance. The maximum difference between the single-gas and mixed-gas hydrogen permeance is less than 8%, and to repeat we observe no systematic trends.

As mentioned above, for a perfect, defect-free Pd membrane, only atomic hydrogen permeates through the Pd metal lattice, with all other gases found in the reformate mixture having negligible solubility and diffusivity; perfect Pd membranes, therefore, should in principle have nearly infinite selectivity towards H<sub>2</sub>. That they do not, is indicative of the fact that other gases permeate through defects and metal lattice imperfections, that are often unavoidable during the preparation of ultra-thin layer Pd membranes. The

hydrogen permeance and selectivity are then two important indicators of the quality of the resulting Pd membranes. Yun and Oyama [33] recently reviewed the performance of Pd and Pd-alloy membranes (prepared via different fabrication methods such as ELP, chemical vapor deposition (CVD), and conventional electroplating (EPD)) in hydrogen separation. They concluded [33] that Pd membranes prepared by the ELP technique are the most promising for practical applications, since ELP allows for easy preparation using simple equipment and various types of supports. Table 2 summarizes the recently published gas separation properties of Pd and Pd-alloy composite membranes prepared by the ELP method, as are the supported membranes used in this study.

Table 3 shows the measured single-gas permeances and calculated separation factors at a temperature of 300 °C for the Pd membrane utilized in the MR experiments, measured first before the experiments were started and then again after the experiments were completed, during which time the membrane had stayed for more than one month (5 weeks) on stream. As Table 3 indicates, the membrane under study possesses a very high hydrogen permeance (see Table 2 for comparison) and selectivity towards the other gases found in the reformate mixture, which is the feed for the WGS reactor. Comparing the hydrogen permeation rates measured before and after the MR experiments, there is a small difference between the hydrogen permeance values measured (~6% decrease), indicative perhaps of small changes occurring on the surface or in the bulk of the metal, most likely due to accumulation of carbon (and/or some yet to be identified impurity) on the membrane surface. The permeation rates of the other gases remained virtually unchanged, indicating that no additional cracks or pinholes were formed as a result of the exposure of the Pd membranes to the WGS environment. These results, therefore, look very promising in terms of long term membrane usage for WGS reaction.

#### 4.2. Reactor studies

A commercial Cu/Zn-based supported LTS catalyst has been used in this study. This type of catalyst has been extensively utilized for the low temperature WGS reaction. Extensive kinetic investigations for an expanded range of pressures, temperatures, and feed compositions with a Cu-Zn supported catalyst of a very similar composition were previously carried out by our group [16]. A reaction rate expression consistent with a Hougen-Watson type surface

**Table 3**

Single-gas permeances measured at 300 °C and calculated separation factors for the Pd membrane before and after the MR experiments.

| Gas             | Before MR exp.                       |                   | After MR exp.                        |                   |
|-----------------|--------------------------------------|-------------------|--------------------------------------|-------------------|
|                 | Permeance (mol/m <sup>2</sup> s bar) | Separation factor | Permeance (mol/m <sup>2</sup> s bar) | Separation factor |
| H <sub>2</sub>  | 0.222 <sup>a</sup>                   | 1                 | 0.208 <sup>a</sup>                   | 1                 |
| CO              | 8.805E-05                            | 2526              | 8.681E-05                            | 2398              |
| CO <sub>2</sub> | 7.068E-05                            | 3147              | 7.192E-05                            | 2894              |
| Ar              | 8.433E-05                            | 2638              | 7.937E-05                            | 2623              |
| N <sub>2</sub>  | 8.185E-05                            | 2718              | –                                    | –                 |
| CH <sub>4</sub> | –                                    | –                 | 8.557E-05                            | 2433              |

<sup>a</sup> The unit for H<sub>2</sub> permeance is (mol/m<sup>2</sup> s bar<sup>0.96</sup>).

**Table 4**  
Hougen–Watson rate parameters [16].

|            |                                   |                            |
|------------|-----------------------------------|----------------------------|
| $E$        | 30.387 (kJ/mol)                   |                            |
| $k$        | 48.16 (mol/g s bar <sup>2</sup> ) |                            |
|            | $\Delta H$ (kJ/mol)               | $k_0$ (bar <sup>-1</sup> ) |
| $K_{H_2}$  | -12                               | 0.0178                     |
| $K_{H_2}$  | -2.42                             | 0.005                      |
| $K_{CO_2}$ | -28                               | 0.0410                     |
| $K_{CO}$   | -0.86                             | 0.0303                     |

mechanism was developed (Eqs. (17) and (18), below), where the various rate parameters are summarized in Table 4.

$$r = \frac{k P_{CO} P_{H_2O} (1 - \beta)}{(1 + K_{H_2} P_{H_2} + K_{CO_2} P_{CO_2} + K_{CO} P_{CO} + K_{H_2O} P_{H_2O})^2} \quad (17)$$

$$\beta = \frac{1}{K_{eq}} \frac{(P_{CO_2} P_{H_2})}{(P_{CO} P_{H_2O})} \quad (18)$$

This rate expression also satisfactorily describes the packed-bed experimental data derived with the catalyst used in this study, as Fig. 6 indicates. Before using in the reactor experiments, the catalyst was activated by passing through the catalyst bed N<sub>2</sub>, as carrier gas, containing hydrogen at compositions and temperatures as recommended by the catalyst manufacturer. The role of hydrogen during the activation process is reducing the copper oxide in the fresh catalyst to copper metal. The activation is complete when the inlet and outlet H<sub>2</sub> concentrations are the same, meaning that the catalyst no longer adsorbs any hydrogen.

Membrane reactor experiments were carried out using the experimental system shown in Fig. 2, utilizing a “commercial size” supported Pd membrane ( $L = 762$  mm, ID = 3.5 mm, OD = 5.7 mm), whose transport characteristics are shown in Table 3. As noted above, the majority of the past studies utilizing Pd membrane reactors for the WGS reaction have used feed compositions very different from what are used industrially. In this study, the feed gas consists of all the species potentially present in the stream exiting the SMR reactor upstream of the WGS reactors. For the membrane reactor experimental data presented here, in particular, the feed had the following composition (in molar ratios) H<sub>2</sub>:CO:CO<sub>2</sub>:CH<sub>4</sub>:H<sub>2</sub>O = 5.22:1:0.48:0.1:2.8, which is chosen to match the calculated equilibrium composition from an SMR reactor operating at a H<sub>2</sub>O/CH<sub>4</sub> = 3,  $T = 850$  °C and  $P = 10$  bar. For the membrane reactor experiments, 30 g of the commercial Cu-Zn/Al<sub>2</sub>O<sub>3</sub> catalyst were diluted with ground quartz glass (enough to fill the reactor volume) and packed in the membrane

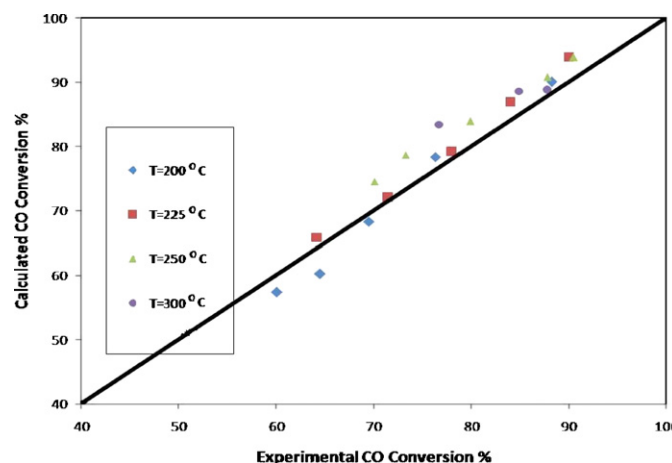


**Fig. 6.** Measured vs. fitted CO conversion data using the Hougen–Watson rate expression [16].

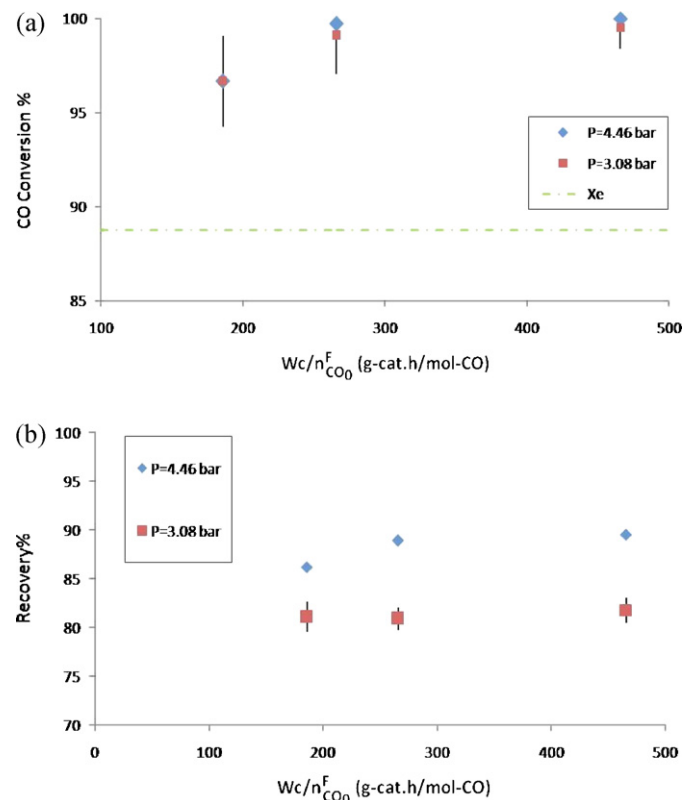


**Fig. 7.** Effect of pressure on (a) CO conversion and (b) H<sub>2</sub> recovery,  $T = 300$  °C and SR = 0.3.

shell-side (the annular volume in between the membrane and the reactor shell). The reactor was maintained under isothermal conditions, and the permeate side was maintained under atmospheric pressure conditions. Steam was utilized as the sweep gas stream.

In the experiments, the effect of varying the feed-side (reactor) pressure and permeate-side sweep ratio (SR = ratio of inlet steam molar flow rate in the permeate side to the inlet molar feed flow rate in the feed-side) on reactor conversion (Eq. (15)) and recovery (Eq. (16)) are studied. Fig. 7a and b shows the CO conversion and H<sub>2</sub> recovery as a function of  $W_c/n_{CO_0}^F$  (weight of undiluted catalyst (g) over the feed molar flow rate of CO (mol/h)), at  $T = 300$  °C and SR = 0.3 for two different operating pressures namely 3.08 and 4.46 bar (the error bars reflect carbon and hydrogen loss or gain due to experimental errors in measuring the flow rates and compositions, and/or possible carbon deposition). Shown in Fig. 7a is also the equilibrium conversion based on the feed composition. Clearly the removal of hydrogen from the reaction mixture has a substantially beneficial effect on reactor conversion. Increasing the  $W_c/n_{CO_0}^F$  and the reactor pressure improves conversion and hydrogen recovery, as expected, with almost complete conversion and hydrogen recovery in excess of 90% being attained. Fig. 8a and b shows the CO conversion and H<sub>2</sub> recovery as a function of  $W_c/n_{CO_0}^F$  for a temperature of 300 °C, a reactor pressure of 4.46 bar and three different sweep ratios, namely SR = 0 (no sweep), SR = 0.1, SR = 0.3 (shown in Fig. 8a is also the calculated equilibrium conversion). As shown in these two figures, increasing the sweep ratio increases both conversion (up to almost complete conversion) and recovery (up to almost 90%), but the effect is stronger for the recovery. Increasing the sweep ratio (as is the case with increasing the feed pressure—see Fig. 7a and b) increases the hydrogen partial pressure difference across the membrane, thus providing a higher driving force for H<sub>2</sub> to diffuse through the membrane. The use of sweep is of particular value for the smaller, and industrially more relevant  $W_c/n_{CO_0}^F$ .

**Table 5**

CO content of the MR H<sub>2</sub> product (permeate side) at two different sets of the experimental conditions.

| T=300 °C, P=4.46 bar no sweep                                 |                        | T=300 °C, P=4.46 bar W <sub>c</sub> /n <sub>CO</sub> <sup>F</sup> = 466 (g-cat h/mol-CO) |                        |
|---|------------------------|--|------------------------|
| W <sub>c</sub> /n <sub>CO</sub> <sup>F</sup> (g-cat.h/mol-CO) | CO concentration (ppm) | Sweep ratio (SR)   | CO concentration (ppm) |
| 466   | 73                     | 0.3  | 59                     |
| 266   | 55                     | 0.1  | 68                     |
| 186   | 41                     | None   | 73                     |

Another important indicator of good MR performance is the purity of the H<sub>2</sub> product, since as noted above fuel cells are very vulnerable to the presence of CO even in small quantities (ppm level). **Table 5** shows the CO content of the H<sub>2</sub> product from the membrane reactor (the stream exiting the permeate side) for a number of different experiments. The CO concentration in the hydrogen product for all experiments reported in **Table 5** remains below 75 ppm, which may be potentially acceptable for few types of PEM fuel cells, as noted previously [6]. For the majority of the PEM fuel cell applications, however, for which CO concentrations below 50 ppm are required, the CO content can be decreased or completely eliminated efficiently with a conventional method such as methanation efficiently, since the low (<75 ppm) CO content in the permeate side stream implies that very little H<sub>2</sub> is going to get consumed during the CO methanation. Furthermore, the presence of trace amounts of CO<sub>2</sub> as well implies that conventional (rather than highly selective) methanation catalysts need to be utilized.

#### 4.3. Scale-up

Due to limitations in terms of the membrane area and the range of pressures that could be employed in our experimental system it was not possible to completely explore, *via* experimentation,

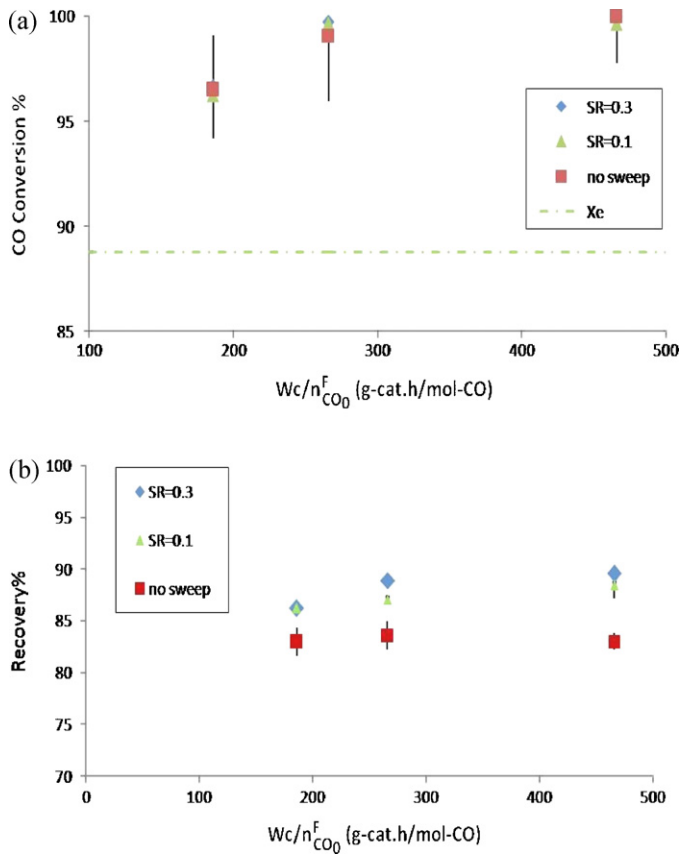


**Fig. 8.** Effect of sweep ratio (SR) on (a) CO conversion and (b) H<sub>2</sub> recovery, T=300 °C and P=4.46 bar.

**Table 6**

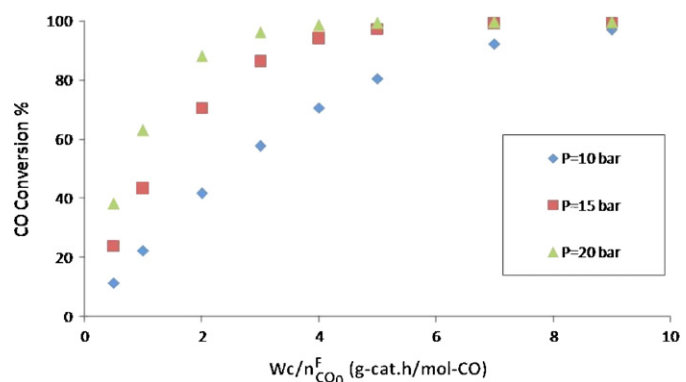
Measured and calculated CO conversion and H<sub>2</sub> recovery for two sets of the experimental conditions.

| W <sub>c</sub> /n <sub>CO</sub> <sup>F</sup> | Conv. (exp.) | Conv. (sim.) | Rec. (exp.) | Rec. (sim.) |
|--|--------------|--------------|-------------|-------------|
| T=300 °C, P=4.46 bar, SR=0.3                 |              |              |             |             |
| 266  | 99.7         | 98.6         | 88.9        | 90.3        |
| T=300 °C, P=4.46 bar, SR=0.1                 |              |              |             |             |
| 266  | 99.6         | 98.2         | 87.1        | 86.9        |

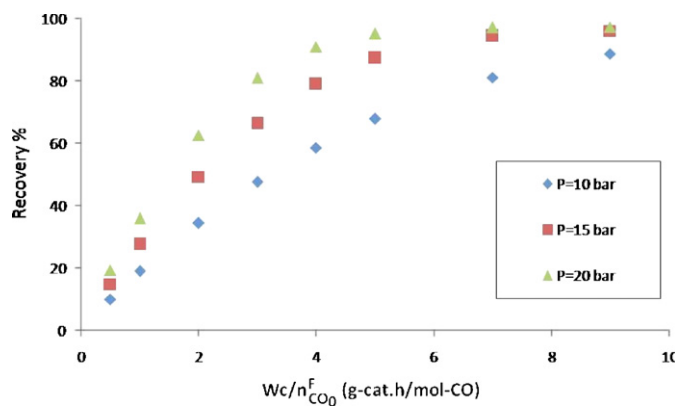
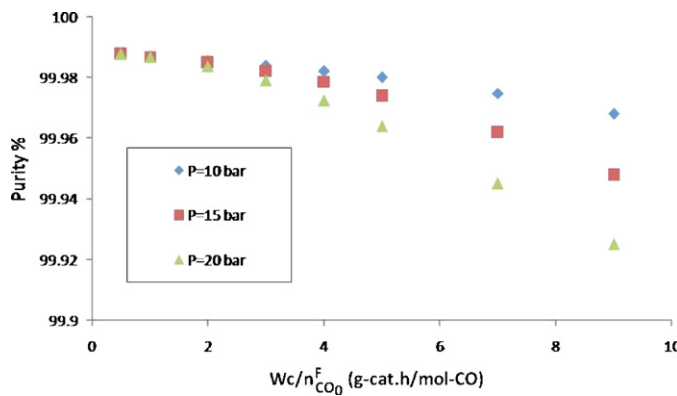
the full range of capabilities of Pd membrane reactors for the WGS reaction. Instead, in this study we have made use of the reaction rate expression in Eq. (17), and the measured single-gas permeances (this based on the experimental observations that mixed-gas permeances do not differ substantially from their single-gas counterparts—see Figs. 4 and 5 and discussion therein) in order to investigate, through simulations utilizing the mathematical model described above, the behavior of the WGS-MR system for conditions more akin to the industrial ones (e.g., in terms of pressure and feed flow rates). The model provides satisfactory agreement with the experimental data, with satisfactory agreement (maximum difference of 6% between the two), see **Table 6**, for example, which presents measured and calculated CO conversions and H<sub>2</sub> recoveries for two sets of experimental conditions.

**Fig. 9** shows the effect of feed pressure on membrane reactor conversion. Increasing reactor pressure has a significant effect on conversion, especially at lower W<sub>c</sub>/n<sub>CO</sub><sup>F</sup>, where it compensates for the decrease in contact time between the gas species and the catalyst due to the high flow rates (in these simulations W<sub>c</sub> is kept constant). These results are very promising, considering the fact that high pressures (~10 bar and higher) and low W<sub>c</sub>/n<sub>CO</sub><sup>F</sup> (<10) are the conditions which are currently applied industrially. Increasing pressure has also the additional beneficial effect in that it increases H<sub>2</sub> recovery (**Fig. 10**) by increasing the partial pressure difference of H<sub>2</sub> across the membrane.

Another very important factor determining good MR performance is the H<sub>2</sub> purity, as previously noted. As **Fig. 11** shows, increasing pressure decreases the H<sub>2</sub> purity due to the fact that it provides a higher driving force for other species, in addition to H<sub>2</sub>, to diffuse through the flaws of the membrane. The effect becomes stronger at higher W<sub>c</sub>/n<sub>CO</sub><sup>F</sup> where the flow rate is lower and the



**Fig. 9.** Effect of pressure on CO conversion, T=300 °C and SR=0.1.

Fig. 10. Effect of pressure on H<sub>2</sub> recovery,  $T=300\text{ }^\circ\text{C}$  and SR = 0.1.Fig. 11. Effect of pressure on H<sub>2</sub> purity,  $T=300\text{ }^\circ\text{C}$  and SR = 0.1.

contact time between the gas and the membrane is higher allowing for a relatively larger fraction of CO to transport through the membrane to the permeate side without undergoing reaction. The purity of the hydrogen product for realistic pressures and  $W_c/F_{CO}$  is very high (above 99.9%), indicating that the use of Pd-MR for industrially relevant conditions is, indeed, promising.

## 5. Summary and conclusions

In this study, an ultra-thin, long, high-performance (in terms of its H<sub>2</sub> permeance and selectivity) supported palladium membrane is used in a membrane reactor system to produce pure hydrogen through the use of the water-gas shift reaction from a gas stream with a simulated reformate composition. The membrane is characterized using single-gas permeation measurements. A Cu-Zn/Al<sub>2</sub>O<sub>3</sub> catalyst is utilized for the WGS reaction. The system performance is investigated under various experimental conditions, namely, different pressures, feed flow rates and sweep ratios. The best performance is obtained at  $T=300\text{ }^\circ\text{C}$ ,  $P=4.46$  bar and the permeate sweep gas ratio = 0.3 with almost complete CO conversion and 90% hydrogen recovery. The product hydrogen purity is always at more than 99.9% with CO concentration of less than 100 ppm. A model is used for further study of the design aspects of the system. It is shown that the Pd membrane reactor system under study is capable of delivering almost complete CO conversion and H<sub>2</sub> recovery at experimental conditions akin to the industrial applications. The membrane exhibits good stability with only a 6% change in the H<sub>2</sub> permeance, and almost no change in the permeation rates of the other gases after being used in the reactor for more than a month under the WGS environment. Hence, it is concluded that the Pd-based WGS-MR is, potentially, a promising system for hydrogen production for fuel cell applications.

## Acknowledgement

The support of the U.S. Department of Energy is gratefully acknowledged.

## Nomenclature

|             |   |
|-------------|---|
| $A^F$       | cross-sectional area for the feed-side ( $\text{m}^2$ )                             |
| $d_p$       | particle diameter in the feed side (m)  |
| $f$         | friction factor   |
| $F_j$       | molar flux for component $j$ ( $\text{mol}/\text{m}^2 \text{ h}$ )                  |
| $F_{H_2}$   | molar flux for hydrogen ( $\text{mol}/\text{m}^2 \text{ h}$ )                       |
| $g_c$       | gravity conversion factor   |
| $G^F$       | superficial mass flow velocity in the feed side ( $\text{g}/\text{m}^2 \text{ h}$ ) |
| ID          | inner diameter of the membrane (m)  |
| $k$         | reaction rate constant ( $\text{mol}/\text{g h bar}^2$ )                            |
| $K_{eq}$    | equilibrium constant  |
| $L$         | length of membrane (m)  |
| $n$         | pressure exponent   |
| $n_j^F$     | molar flow rate for component $j$ in the feed side (mol/h)                          |
| $n_{H_2}^F$ | molar flow rate for hydrogen in the feed side (mol/h)                               |
| $n_j^P$     | molar flow rate for component $j$ in the permeate side (mol/h)                      |
| $n_{H_2}^P$ | molar flow rate for hydrogen in the permeate side (mol/h)                           |
| $N_{Re}^F$  | Reynolds number for the feed-side   |
| OD          | outer diameter of the membrane (m)  |
| $P_j$       | partial pressure for component $j$ (bar)  |
| $P^F$       | feed-side pressure (bar)  |
| $P_j^F$     | partial pressure for component $j$ in the feed-side (bar)                           |
| $P_{H_2}^F$ | partial pressure for hydrogen in the feed side (bar)                                |
| $P^P$       | permeate side pressure (bar)  |
| $P_j^P$     | partial pressure for component $j$ in the permeate side (bar)                       |
| $P_{H_2}^P$ | partial pressure for hydrogen in the permeate side (bar)                            |
| $r$         | overall reaction rate expression (mol/g h)  |
| $Re_{H_2}$  | hydrogen recovery, defined by Eq. (16)  |
| SR          | steam sweep gas ratio ( $\sum n_{j_0}^P / \sum n_{j_0}^F$ )                         |
| $T$         | temperature   |
| $u^F$       | superficial flow velocity on the feed side (m/h)                                    |
| $U_j$       | membrane permeance for component $j$ ( $\text{mol}/\text{m}^2 \text{ h bar}^n$ )    |
| $U_{H_2}$   | H <sub>2</sub> permeance (mol/m <sup>2</sup> h bar <sup>n</sup> )                   |
| $V$         | reactor volume variable (m <sup>3</sup> )   |
| $W_C$       | weight of the catalyst (g)  |
| $X_{CO}$    | carbon monoxide conversion, defined by Eq. (15)                                     |

**Greek letters**

|                 |  |
|-----------------|--|
| $\alpha_m$      | membrane area per feed side reactor volume ( $\text{m}^2/\text{m}^3$ ) |
| $\beta$         | equilibrium coefficient  |
| $\beta_c$       | fraction of solid volume occupied by catalyst                          |
| $\varepsilon_v$ | bed porosity in the feed side  |
| $\mu^F$         | viscosity of the fluid (g/m h)   |
| $\rho^F$        | average density of the fluid (g/m <sup>3</sup> )                       |
| $\rho^c$        | catalyst density (g/m <sup>3</sup> )                                   |
| $v_j$           | stoichiometric coefficient for component $j$                           |

**Subscripts**

|      |                    |
|------|--------------------|
| O    | entrance condition |
| eq   | equilibrium        |
| exit | exit condition     |
| j    | chemical species   |

**Superscripts**

|   |                     |
|---|---------------------|
| F | feed (reactor) side |
| P | permeate side       |

**References**

- [1] [http://en.wikipedia.org/wiki/Proton\\_exchange\\_membrane\\_fuel\\_cell](http://en.wikipedia.org/wiki/Proton_exchange_membrane_fuel_cell).
- [2] [http://www1.eere.energy.gov/hydrogenandfuelcells/fuelcells/fc\\_types.html](http://www1.eere.energy.gov/hydrogenandfuelcells/fuelcells/fc_types.html).
- [3] M.N. Islam, M. Dixon, Review of various process routes for hydrogen production, *Fuel Energy Abstr.* 45 (2004) 254.
- [4] J.D. Holladay, J. Hu, D.L. King, Y. Wang, An overview of hydrogen production technologies, *Catal. Today* 139 (2009) 244–260.
- [5] T. Okada, H. Yano, C. Ono, Novel CO tolerant anode catalysts for PEFC based on platinum and organic metal complexes, *J. New Mater. Electrochim. Syst.* 10 (2007) 129–134.
- [6] E. Yoo, T. Okada, T. Kizuka, J. Nakamura, Effect of various carbon substrate materials on the CO tolerance of anode catalysts in polymer electrolyte fuel cells, *Electrochemistry* 75 (2007) 146–148.
- [7] J. Shu, B.P.A. Grandjean, S. Kaliaguine, Methane steam reforming in asymmetric Pd- and Pd Ag/porous SS membrane reactors, *Appl. Catal. A: Gen.* 119 (1994) 305–325.
- [8] Y. Chen, Y. Wang, H. Xu, G. Xiong, Efficient production of hydrogen from natural gas steam reforming in palladium membrane reactor, *Appl. Catal. B: Environ.* 81 (2008) 283–294.
- [9] A. Basile, G. Chiappetta, S. Tosti, V. Violante, Experiments and simulation of both Pd and Pd/Ag for a water gas shift membrane reactor, *Sep. Purif. Technol.* 25 (2001) 549–571.
- [10] O. Iyoha, R. Enick, R. Killmeyer, B. Howard, B. Morreale, M. Ciocco, Wall-catalyzed water-gas shift reaction in multi-tubular Pd and 80 wt% Pd–20 wt% Cu membrane reactors at 1173 K, *J. Membr. Sci.* 298 (2007) 14–23.
- [11] Y. Bi, H. Xu, W. Li, A. Goldbach, Water-gas shift reaction in a Pd membrane reactor over Pt/Ce<sub>0.6</sub>Zr<sub>0.4</sub>O<sub>2</sub> catalyst, *Int. J. Hydrogen Energy* 34 (2009) 2965–2971.
- [12] D. Mendes, V. Chibante, J.M. Zheng, S. Tosti, F. Borgognoni, A. Mendes, L.M. Madeira, Enhancing the production of hydrogen via water gas shift reaction using Pd-based membrane reactors, *Int. J. Hydrogen Energy* 35 (2010) 12596–12608.
- [13] G. Barbieri, A. Brunetti, G. Tricoli, E. Drioli, An innovative configuration of a Pd-based membrane reactor for the production of pure hydrogen: experimental analysis of water gas shift, *J. Power Sources* 182 (2008) 160–167.
- [14] S. Giessler, L. Jordan, J.C. Diniz da Costa, G.Q.M. Lu, Performance of hydrophobic and hydrophilic silica membrane reactors for the water gas shift reaction, *Sep. Purif. Technol.* 32 (2003) 255–264.
- [15] A. Harale, H.T. Hwang, P.K.T. Liu, M. Sahimi, T.T. Tsotsis, Experimental studies of a hybrid adsorbent-membrane reactor (HAMR) system for hydrogen production, *Chem. Eng. Sci.* 62 (2007) 4126–4137.
- [16] A. Harale, H.T. Hwang, P.K.T. Liu, M. Sahimi, T.T. Tsotsis, Design aspects of the cyclic hybrid adsorbent-membrane reactor (HAMR) system for hydrogen production, *Chem. Eng. Sci.* 65 (2010) 427–435.
- [17] M. Abdollahi, J. Yu, P.K.T. Liu, R. Ciora, M. Sahimi, T.T. Tsotsis, Hydrogen production from coal-derived sygas using a catalytic membrane reactor based process, *J. Membr. Sci.* 363 (2010) 160–169.
- [18] D. Jansen, J.W. Dijkstra, R.W. van den Brink, T.A. Peters, M. Stange, R. Bredesen, A. Goldbach, H.Y. Xu, A. Gottschalk, A. Doukelis, Hydrogen membrane reactors for CO<sub>2</sub> capture, *Energy Procedia* 1 (2009) 253–260.
- [19] S.K. Gade, P.M. Thoenand, J.D. Way, Unsupported palladium alloy foil membranes fabricated by electroless plating, *J. Membr. Sci.* 316 (2008) 112–118.
- [20] H.T. Hwang, A. Harale, P.K.T. Liu, M. Sahimi, T.T. Tsotsis, A membrane-based reactive separation system for CO<sub>2</sub> removal in a life support system, *J. Membr. Sci.* 315 (2008) 116–124.
- [21] T.L. Ward, T. Dao, Model of hydrogen permeation behavior in palladium membranes, *J. Membr. Sci.* 153 (1999) 211–231.
- [22] R.C. Hurlbert, J.O. Konecny, Diffusion of hydrogen through palladium, *J. Chem. Phys.* 34 (1961) 655–658.
- [23] B.D. Morreale, M.V. Ciocco, R.M. Enick, B.I. Morsi, B.H. Howard, A.V. Cugini, K.S. Rothenberger, The permeability of hydrogen in bulk palladium at elevated temperatures and pressures, *J. Membr. Sci.* 212 (2003) 87–97.
- [24] S. Yan, H. Maeda, K. Kusakabe, S. Morooka, Thin palladium membrane formed in support pores by metal-organic chemical-vapor-deposition method and application to hydrogen separation, *Ind. Eng. Chem. Res.* 33 (1994) 616–622.
- [25] A. Harale, A hybrid adsorbent-membrane reactor (HAMR) system for hydrogen production, Ph.D. dissertation, University of Southern California, Los Angeles, CA, 2008.
- [26] H.T. Hwang, A study of the application of membrane-based reactive separations to the carbon dioxide methanation, Ph.D. dissertation, University of Southern California, Los Angeles, CA, 2009.
- [27] H. Amandusson, L.G. Ekedahl, H. Dannetun, Hydrogen permeation through surface modified Pd and Pd–Ag membranes, *J. Membr. Sci.* 193 (2001) 35–47.
- [28] S. Uemiya, N. Sato, H. Ando, E. Kikuchi, The water gas shift reaction assisted by a palladium membrane reactor, *Ind. Eng. Chem. Res.* 30 (1991) 585–589.
- [29] Y. Guo, G. Lu, Y. Wang, R. Wang, Preparation and characterization of Pd–Ag/ceramic composite membrane and application to enhancement of catalytic dehydrogenation of isobutene, *Sep. Purif. Technol.* 32 (2003) 271–279.
- [30] E. Gobina, R. Hughes, Ethane dehydrogenation using a high-temperature catalytic membrane reactor, *J. Membr. Sci.* 90 (1994) 11–19.
- [31] F. Roa, J.D. Way, Influence of alloy composition and membrane fabrication on the pressure dependence of the hydrogen flux of palladium-copper membranes, *Ind. Eng. Chem. Res.* 42 (2003) 5827–5835.
- [32] S.H. Israni, M.P. Harold, Methanol steam reforming in Pd–Ag membrane reactors: effects of reaction system species on transmembrane hydrogen flux, *Ind. Eng. Chem. Res.* 49 (2010) 10242–10250.
- [33] S. Yun, S.T. Oyama, Correlations in palladium membranes for hydrogen separation: a review, *J. Membr. Sci.* (2011), doi:10.1016/j.memsci.2011.03.057.
- [34] X. Zhang, G. Xiong, W. Yang, A modified electroless plating technique for thin dense palladium composite membranes with enhanced stability, *J. Membr. Sci.* 314 (2008) 226–237.
- [35] D. Tanaka, M. Tanco, T. Nagase, J. Okazaki, Y. Yakui, F. Mizukami, T. Suzuki, Preparation of pore-fil type Pd–YSZ-gamma-Al<sub>2</sub>O<sub>3</sub> composite membrane supported on alpha-Al<sub>2</sub>O<sub>3</sub> tube for hydrogen separation, *J. Membr. Sci.* 320 (2008) 436–441.
- [36] B. Nair, J. Choi, M.P. Harold, Electroless plating and permeation features of Pd and Pd/Ag hollow fiber composite membranes, *J. Membr. Sci.* 288 (2007) 67–84.
- [37] B. Nair, M.P. Harold, Pd encapsulated and nanopore hollow fiber membranes: synthesis and permeation studies, *J. Membr. Sci.* 290 (2007) 182–195.
- [38] Y. Guo, X. Zhan, H. Deng, X. Wang, Y. Wang, J. Qiu, J. Wang, K.L. Yeung, A novel approach for the preparation of highly stable Pd membrane on macroporous α-Al<sub>2</sub>O<sub>3</sub> tube, *J. Membr. Sci.* 362 (2010) 241–248.